Solution Structures of the Ca^{2+}-free and Ca^{2+}-bound C_2A Domain of Synaptotagmin I: Does Ca^{2+} Induce a Conformational Change?†

Xuguang Shao,‡ Imma Fernandez,‡ Thomas C. Südhof,§ and Josep Rizo*,‡

Departments of Biochemistry, Pharmacology, and Molecular Genetics, and Howard Hughes Medical Institute, University of Texas Southwestern Medical Center at Dallas, 5323 Harry Hines Boulevard, Dallas, Texas 75235

Received July 24, 1998

ABSTRACT: C_2 domains are widespread Ca^{2+}-binding modules that are particularly abundant in proteins involved in membrane traffic and signal transduction. The C_2A domain of synaptotagmin I is believed to play a key role in neurotransmitter release through its Ca^{2+}-dependent interactions with syntaxin and phospholipids. Elucidating the structural consequences of Ca^{2+} binding to the C_2A domain is critical for understanding its mechanism of action and for models of the functions of other C_2 domains. We have determined the solution structure of the Ca^{2+}-free and Ca^{2+}-bound forms of the C_2A domain of synaptotagmin I by NMR spectroscopy. Our data represent the first structure determination of a C_2 domain in its Ca^{2+}-free and Ca^{2+}-bound forms. Three Ca^{2+} ions were included in the Ca^{2+}-bound structure, yielding a Ca^{2+}-binding motif that involves five aspartate side chains and one serine side chain. Ca^{2+} immobilizes the structure of the C_2A domain but does not produce a significant conformational change from a well-defined conformation to another. Thus, the mechanism of action of the C_2A domain of synaptotagmin I is different from that used by Ca^{2+}-binding proteins of the EF-hand family. The main effect of Ca^{2+} binding on the C_2A domain is to change its electrostatic potential rather than its structure. These results support a model whereby the C_2A domain functions as an electrostatic switch in neurotransmitter release. The similarity between the structures of the synaptotagmin I C_2A domain and the PLC-δ1 C_2 domain suggests that the latter binds four Ca^{2+} ions and acts by a similar mechanism. This mechanism may also be valid for other C_2 domains that share the unusual ability to bind multiple Ca^{2+} ions in a tight cluster at the tip of the domain.

Ca^{2+}-evoked synaptic vesicle exocytosis initiates neurotransmission. The synaptic vesicle protein synaptotagmin I is essential for fast synaptic vesicle exocytosis (*1*) and is probably the main Ca^{2+} receptor in this process (reviewed in refs *2* and *3*). The sequence of synaptotagmin I is characterized by the presence of two consecutive repeats that are homologous to the C_2 domain of protein kinase C (PKC) (*4*−*6*). The two C_2 domains span most of the cytoplasmic region of synaptotagmin I and are believed to constitute the executive center of the protein. The first C_2 domain (C_2A domain[1]) binds phospholipids in a Ca^{2+}-dependent manner similar to that of the full-length protein (*7*, *8*). The cooperativity and divalent cation selectivity of this interaction parallel those observed in synaptic vesicle exocytosis. The C_2A domain also exhibits Ca^{2+}-dependent binding to syntaxin (*9*−*11*), a plasma membrane protein that is widely believed to be a key component of the exocytotic machinery (reviewed in refs *2* and *12*). The Ca^{2+} concentrations required for this interaction are similar to those that trigger neurotransmitter release (*13*). All of these observations indicate that the C_2A domain of synaptotagmin I plays a key role in Ca^{2+}-evoked exocytosis.

Since the C_2 domain was first identified as a conserved region in the classical isoforms of PKC (*14*), this protein module has been found in a large number of proteins (reviewed in refs *15*−*17*), with close to 100 C_2 domain sequences currently in the data banks. As the number of C_2 domain-containing proteins identified increases, so does the diversity of their functions. Many C_2 domains share a common characteristic, the ability to bind Ca^{2+}. This property has been most often manifested by Ca^{2+}-dependent phospholipid binding, as in the case of the synaptotagmin I C_2A domain. Elucidating how Ca^{2+} regulates the interactions of the C_2A domain thus not only is important to understand the function of synaptotagmin I but can also provide a model for the mechanisms of action of many other C_2 domains.

The structure of the C_2A domain of synaptotagmin I has been determined by X-ray crystallography and consists of a compact β-sandwich formed by two four-stranded β-sheets, with loops emerging at the top and the bottom of the sandwich (*18*). X-ray diffraction analysis of the phosphoinositide-specific phospholipase C-δ1 (PLC-δ1) showed that its C_2 domain adopts a very similar structure but with a

* Corresponding author. Tel: 214-648-9026. Fax: 214-648-8673. E-mail: jose@arnie.swmed.edu.

† Support provided by a fellowship from the Ministerio de Educacion y Ciencia of Spain (I.F.), a joint grant from the United Cerebral Palsy Research and Educational Foundation and the William Randolph Hearst Foundation (J.R.), and NIH Grant NS33731 (to J.R.).

‡ Departments of Biochemistry and Pharmacology.

§ Department of Molecular Genetics and Howard Hughes Medical Institute.

[1] Abbreviations: C_2A domain, first C_2 domain of synaptotagmin I; $cPLA_2$, cytoplasmic phospholipase A_2; DQF−COSY, double-quantum filtered correlation spectroscopy; HMQC, heteronuclear multiple-quantum correlation; HSQC, heteronuclear single-quantum correlation; NOE, nuclear Overhauser effect; NOESY, NOE spectroscopy; PLC, phosphoinositide-specific phospholipase C; PKC, protein kinase C; rms, root-mean-square; TOCSY, total correlation spectroscopy.

10.1021/bi981789h CCC: $15.00
Published on Web 10/26/1998

different topology that results from a circular permutation of the β-strands (*19*−*21*). The crystal structure of the C_2 domain of cytosolic phospholipase A_2 ($cPLA_2$) is also very similar and has the topology of the PLC-δ1 C_2 domain (*22*). These studies have laid the foundation to study the functions of C_2 domains on three-dimensional structural grounds. However, it has been difficult so far to obtain crystal structures for a given C_2 domain in its Ca^{2+}-free and fully Ca^{2+}-saturated forms, which has hindered the determination of complete Ca^{2+}-binding modes and/or the analysis of structural changes caused by Ca^{2+} binding.

Diffusion of 100 μM Ca^{2+} into crystals of the synaptotagmin I C_2A domain revealed binding of one Ca^{2+} ion at a region formed by the top loops of the domain (which we will refer to as loops 1−3), but higher Ca^{2+} concentrations could not be reached due to fraying of the crystals. Using NMR spectroscopy, we showed that the synaptotagmin I C_2A domain and the PKC-β1 C_2 domain bind at least two Ca^{2+} ions in solution (*23*), and later demonstrated that the synaptotagmin I C_2A domain binds a total of three Ca^{2+} ions in a tight cluster at the same region of the domain (*24*). All three Ca^{2+} ions are required for the Ca^{2+}-dependent interactions of the C_2A domain with syntaxin and phospholipids (*24*, *25*). For the PLC-δ1 C_2 domain, binding of two Ca^{2+} ions was observed after diffusion of 1 mM Ca^{2+} into PLC-δ1 crystals, but it is possible that saturation of this C_2 domain involves binding of three Ca^{2+} ions (*21*) or even four (*24*). Two Ca^{2+} binding sites were observed in the C_2 domain of $cPLA_2$, which was cocrystallized in the presence of Ca^{2+} but did not crystallize in its absence (*22*).

Determination of the structural consequences of Ca^{2+} binding to C_2 domains is critical to understand how they execute their functions. A Ca^{2+}-induced conformational change is a natural expectation, and mechanisms whereby loops 1 and 3 close (*26*) or open (*20*, *27*) upon Ca^{2+} binding have been proposed. However, no conclusive evidence for such mechanisms has been described. An alternative view suggested by NMR analysis of the synaptotagmin I C_2A domain and its Ca^{2+}-dependent interaction with syntaxin postulates that this interaction is driven by a Ca^{2+}-induced change in the electrostatic potential of the C_2A domain and is stabilized through partial coordination of Ca^{2+} by syntaxin (*11*, *23*, *24*). Ca^{2+}-dependent phospholipid binding is likely to occur by a similar mechanism (*25*). The question thus arises whether Ca^{2+} binding induces a conformational change in C_2 domains, or if they act by a different mechanism. To answer this question, we have solved the structure in solution of the C_2A domain of synaptotagmin I. Analysis in solution has allowed us to compare for the first time the structure of a C_2 domain in its Ca^{2+}-free and fully Ca^{2+}-saturated forms. We show that Ca^{2+} binding stabilizes the structure of the C_2A domain rather than causing a change from a well-defined conformation to another. These results support the proposal that it is the change in electrostatic potential caused by Ca^{2+} binding, and possibly the presence of empty Ca^{2+} coordination sites, that changes the affinity of C_2 domains for target molecules upon Ca^{2+} binding.

RESULTS

Ca^{2+} Stabilizes the Structure of the C_2A Domain. The structure of the C_2A domain of synaptotagmin I in the presence of either 0.2 mM EGTA or 30 mM Ca^{2+} was analyzed by multidimensional NMR spectroscopy. The resonance assignments for both the Ca^{2+}-free and Ca^{2+}-bound forms of the C_2A domain have been described previously (*28*). The conformational behavior of both forms was initially compared through analysis of NOEs assigned in 2D NOESY and 3D ^{1}H-^{15}N NOESY−HMQC spectra, as well as of $^3J_{HN\alpha}$ coupling constants and H/D exchange rates. The data obtained for both forms were in general very similar and consistent with the crystal structure of the Ca^{2+}-free C_2A domain. These included a large number of interstrand backbone−backbone NOEs that delineate the topology of the two four-stranded antiparallel β-sheets. Interruption of the NOE patterns characteristic of antiparallel β-structure, including the observation of strong sequential HN/HN NOEs in the middle of β-strands, defined four β-bulges that are characteristic of the C_2 domain fold (*18*). The β-sheet architecture of the domain and the good dispersion of chemical shifts facilitated the assignment of long-range NOEs involving side-chain protons, which, together with the backbone−backbone NOEs, defined unambiguously the overall tertiary structure of the C_2A domain.

Significant differences between the NMR data obtained for the Ca^{2+}-free and Ca^{2+}-bound forms of the C_2A domain were only observed in the Ca^{2+}-binding region formed by the three loops that connect β-strands at the top of the domain. A considerable number of long-range NOEs between protons in this region that were observed for the Ca^{2+}-bound form had substantially smaller intensities or were absent in the data obtained for the Ca^{2+}-free C_2A domain. Interestingly, the data corresponding to the Ca^{2+}-bound form were consistent with the interproton distances that can be predicted from the Ca^{2+}-free crystal structure, but the small NOE intensities observed in the absence of Ca^{2+} were not. This is illustrated by the contour plots shown in Figure 1. Particularly notable are the weak intensities of the H237 Hϵ1/F231 Hδ and T176 HN/A170 Hβ NOEs observed in the Ca^{2+}-free C_2A domain (Figure 1A,C); from the Ca^{2+}-free crystal structure, these NOEs are predicted to be strong, as observed for the Ca^{2+}-bound C_2A domain in solution (Figure 1B,D). The H237 Hϵ1/F231 Hϵ, H237 Hϵ1/Y180 Hϵ, and T176 HN/L202 Hδ2 cross-peaks constitute additional examples of NOEs observed for the Ca^{2+}-bound C_2A domain with intensities that are consistent with the crystal structure of the Ca^{2+}-free C_2A domain but had lower intensities or were absent for the Ca^{2+}-free C_2A domain in solution (Figure 1). Note, however, that intraresidue NOEs such as that between T176 HN and T176 Hγ had similar intensities in the Ca^{2+}-free and Ca^{2+}-bound data (Figure 1C,D). A careful analysis of the NOE data obtained for the Ca^{2+}-free and Ca^{2+}-bound C_2A domains did not reveal any NOE intensity significantly higher than expected from the crystal structure.

The picture that emerges from these observations is that the solution structure of the C_2A domain, whether in its Ca^{2+}-free or Ca^{2+}-bound state, is very similar to the crystal structure but the conformation of the Ca^{2+}-binding loops is unstable in the absence of Ca^{2+}. Thus, structural fluctuations in the region decrease the percentage of time that protons involved in some of the long-range NOEs spend close to each other, yielding smaller NOE intensities. A higher flexibility at the Ca^{2+}-binding region in the absence of Ca^{2+} is also supported by amide H/D exchange rates. Since the

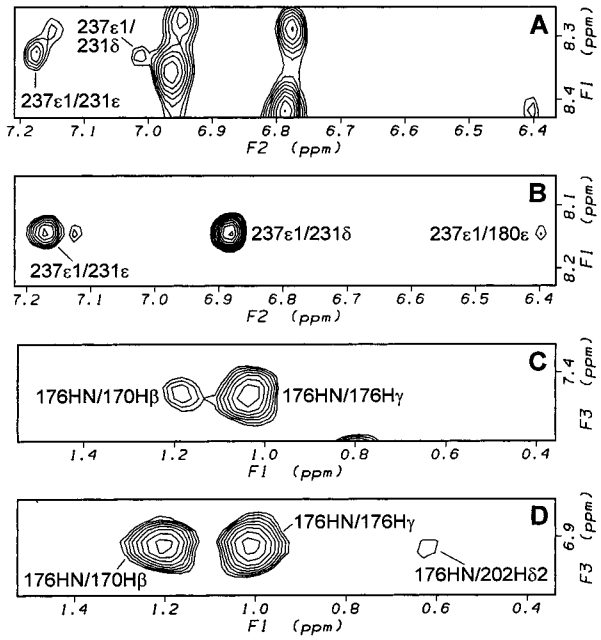

FIGURE 1: Ca^{2+} binding stabilizes the structure of the C_2A domain. Contour plots of 2D NOESY (A, B) and 3D NOESY−HMQC (C, D) spectra containing long-range NOEs with substantially lower intensities for the Ca^{2+}-free than the Ca^{2+}-bound C_2A domain are shown. A and C correspond to the Ca^{2+}-free C_2A domain and B and D to the Ca^{2+}-bound C_2A domain. The contour plots of the 3D NOESY−HMQC spectra correspond to planes taken at the ^{15}N chemical shift of the T176 HN (111.1 and 108.5 ppm for the Ca^{2+}-free and Ca^{2+}-bound C_2A domains, respectively). The cross-peaks discussed in the text have been labeled using the residue numbers and the designators for the heavy atoms bearing the corresponding protons. The interproton distances (Å) corresponding to these NOEs predicted from the Ca^{2+}-free crystal structure (*18*), representing methyl groups by pseudoatoms, are the following: H237 Hϵ1/F231 Hϵ, 2.93; H237 Hϵ1/F231 Hδ, 2.58; H237 Hϵ1/Y180 Hϵ, 4.14; T176 HN/A 170 Hβ*, 3.79; T176 HN/T176 Hγ*, 4.13; and T176 HN/L202 Hδ2*, 5.81.

Ca^{2+}-binding loops are highly exposed to the solvent, many of their amide protons are not protected from exchange. However, buried amide groups at the base of this region that are hydrogen bonded in the crystal structure are substantially more protected from exchange in the Ca^{2+}-bound C_2A domain than in the Ca^{2+}-free form. These include the amide groups of residues L171, H198, K200, T201, N203, D230, and F231. The heteronuclear ^1H-^{15}N NOEs in the Ca^{2+}-binding loops are slightly smaller in the Ca^{2+}-free C_2A domain (ca. 0.5−0.6) than in the Ca^{2+}-bound C_2A domain (ca. 0.7−0.8), supporting the existence of flexibility in the absence of Ca^{2+} but indicating that the flexibility is limited.

Solution Structure of the Ca^{2+}-Free C_2A Domain. To ensure that the NMR data obtained for the Ca^{2+}-free C_2A domain indeed defines a structure analogous to the crystal structure, we calculated 43 structures by simulated annealing (*29*) using a set of 1211 restraints derived from the NMR data acquired in the absence of Ca^{2+}. A backbone superposition of the 10 structures with the lowest restraint violations is shown in Figure 2A. The structure of most of the molecule is well-defined, particularly in the β-sheets. The average backbone rms deviation among the structures is 1.53 Å for residues 143−263 and decreases to 1.13 Å when excluding the Ca^{2+}-binding loops (loops 1 and 3 which correspond to residues 170−180 and 230−240). Certain conformations appear to predominate in these loops, but

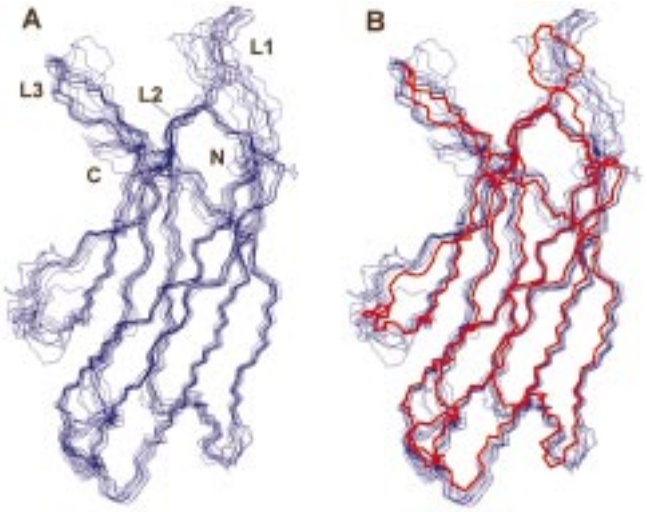

FIGURE 2: Solution structure of the Ca^{2+}-free C_2A domain. (A) Backbone superposition of the 10 simulated annealing structures with the lowest restraint violations generated by superimposing the backbone of residues 143−263 of each structure with the average structure. The positions of loops 1−3 (labeled L1−L3) and of the N- and C-termini are indicated. The solution structures were calculated using a total of 1211 restraints, which included 1025 NOE distance restraints (244 intraresidue, 318 sequential [$|i - j| = 1$), 88 short-range ($|i - j| = 2-4$), 375 long-range ($|i - j| > 4$)], 114 hydrogen bond distance restraints, and 72 dihedral angle restraints. There were no systematic distance restraint violations above 0.3 Å and no dihedral angle violations larger than 5°. (B) Comparison of the 10 simulated annealing structures (thin blue lines) with the Ca^{2+}-free crystal structure (thick red lines). The 10 simulated annealing structures were superimposed as in A, and the backbone of residues 143−263 of the X-ray structure was superimposed to the average solution structure.

substantially different conformations are equally compatible with the NMR data. As shown in Figure 2B, the well-defined regions of the 10 simulated annealing structures calculated for the Ca^{2+}-free C_2A domain in solution superimpose well with the crystal structure. The average backbone rms deviation between the 10 structures and the X-ray structure is 1.46 Å for residues 143−163 and 1.10 Å excluding the Ca^{2+}-binding loops. These values are similar to the deviations observed among the NMR structures. The major differences are observed in the Ca^{2+}-binding loops, particularly in loop 1. However, these differences and the structural heterogeneity observed in the loops are in part a direct consequence of the low intensity or absence of several long-range NOEs that would help define better the conformation in this region. Given the felixibilty of the loops in the absence of Ca^{2+} and the availability of a high-resolution crystal structure that can be taken as a representative of the most populated conformation in solution, we did not attempt to refine the solution structure of the Ca^{2+}-free C_2A domain any further.

Solution Structure of the Ca^{2+}-Bound C_2A Domain. The 2D NOESY and 3D ^1H-^{15}N NOESY−HMQC data, $^3J_{HN\alpha}$ coupling constants, and H/D exchange data obtained for the Ca^{2+}-bound C_2A domain define its structure to an extent similar to that described above for the Ca^{2+}-free form, with some better convergence in the Ca^{2+}-binding loops due to the presence of more and stronger long-range NOEs in this region. Since our main goal was to analyze in detail the structural consequences of Ca^{2+} binding to the C_2A domain, we sought to increase the accuracy of the Ca^{2+}-bound

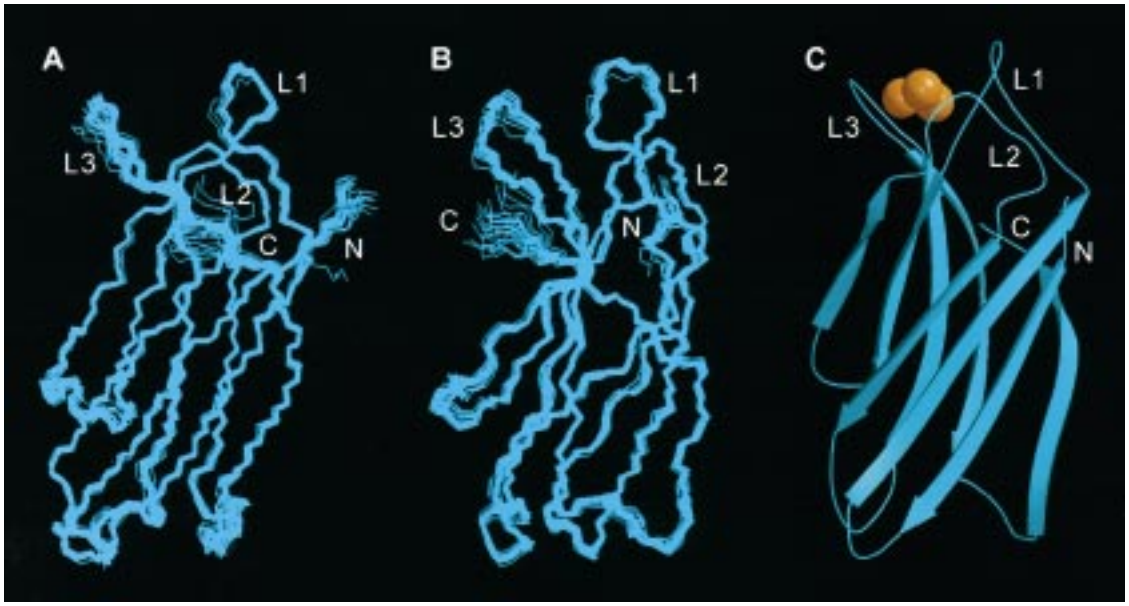

FIGURE 3: Solution structure of the Ca^{2+}-bound C_2A domain. (A, B) Backbone superposition of the 20 simulated annealing structures with lowest violations from experimental restraints, shown from two different angles. The backbone of residues 143−263 of the 20 structures was superimposed with the average structure. (C) Ribbon diagram of the average of the 20 structures with the three bound Ca^{2+} ions shown as orange spheres. This diagram was generated with the programs MOLSCRIPT (*57*) and Raster-3D (*58*). The positions of loops 1−3 (labeled L1−L3) and the N- and C-termini are indicated. Coordinates have been deposited in the Brookhaven Protein Data Bank under accession number 1byn.

structure by obtaining additional restraints from a 4D ^{1}H-^{13}C,^{1}H-^{13}C HMQC−NOESY−HMQC experiment. Initial simulated annealing structures incorporating all data were calculated without including Ca^{2+} ions. The addition of restraints to include Ca^{2+} ions (see below) had very minor effects on the structures obtained. Figure 3 shows a superposition of the final 20 structures of the Ca^{2+}-bound C_2A domain with the lowest restraint violations, and a ribbon representation of the average structure. Table 1 summarizes the structural statistics. The structures are compared with the Ca^{2+}-free crystal structure in Figure 4.

The quality of the structures of the Ca^{2+}-bound C_2A domain obtained is demonstrated by the low rms deviations from the NMR derived restraints, particularly those involving long-range NOEs, and the low deviations from idealized covalent geometry (Table 1). In addition, 98.8% of the residues were in the most favored and additionally allowed regions of the Ramachandran map as calculated with the program PROCHECK (*30*). The solution structure of the Ca^{2+}-bound C_2A domain is very well-defined, with a 0.49 Å average backbone rms deviation among residues 143−263 of the 20 structures; the corresponding average rms deviation for all heavy atoms is 1.05 Å. The backbone and all heavy-atom rms deviations for the Ca^{2+}-binding loops after superimposing only the residues in the loops (residues 170−180 and 230−240) are 0.42 and 1.04 Å, respectively. Therefore, the conformation of these loops is also well-defined although some hinge motions with respect to the β-sandwhich part of the molecule may exist (see Figure 3A,B).

Comparison of the Ca^{2+}-bound solution structures with the Ca^{2+}-free crystal structure (Figure 4) shows a remarkable similarity even in the Ca^{2+}-binding region. The average backbone rms deviation with respect to the X-ray structure is 0.73 Å for residues 143−263 and 0.72 Å for the Ca^{2+}-binding loops. When all heavy atoms in the loops are compared, the average rms deviation with respect to the crystal structure is 1.66 Å, reflecting some heterogeneity in side-chain conformations and the fact that some side chains rotate in order to bind Ca^{2+}. Slight differences in the backbone conformation are observed for loop 1, but the maximum distance deviation between a backbone atom in the average Ca^{2+}-bound solution structure and the same atom in the Ca^{2+}-free crystal structure after superimposing the backbone of residues 143−263 is 1 Å. Considering that some flexibility may remain in this loop since there are two glycine residues at its tip, it is likely that the differences observed are within experimental error. Note that substantially larger differences are observed in this loop when different crystal structures of PLC-δ1 (*19*−*21*) are compared. Overall, our results demonstrate that the Ca^{2+}-bound solution structure is almost identical to the Ca^{2+}-free crystal structure. Thus, Ca^{2+} does not induce a conformational change from a well-defined conformation to another but rather causes immobilization of the structure at the Ca^{2+}-binding region of the domain.

Ca^{2+}-Binding Mode of the C_2A Domain. Our analysis of the Ca^{2+}-binding mode of the C_2A domain using Mn^{2+}-induced relaxation experiments, site-directed mutagenesis, and Ca^{2+} titrations monitored by ^{1}H-^{15}N HSQC demonstrated binding of three Ca^{2+} ions (which we refer to as Ca1, Ca2, and Ca3), and revealed side chains that were essential for the binding of each individual Ca^{2+} ion (*24*). Restraints to include the three Ca^{2+} ions in the solution structures described above were added in a progressive fashion. We first included restraints between each Ca^{2+} ion and the corresponding essential side chains (D178 for Ca1; D232 and D238 for Ca2; D232, S235, and D238 for Ca3). From structures obtained with these restraints, additional ligands for each Ca^{2+} ion became obvious because of their proximity to the ions (<3 Å) in all or almost all structures obtained. Addition of restraints between these ligands and the corre-

Table 1: Structural Statistics for the Final 20 Simulated Annealing Structures of the Ca^{2+}-Bound C_2A Domain[a]

Average rms Deviations from Experimental Restraints	
NOE distances all (1287) (Å)	0.011
intraresidue (370)	0.017
sequential ($\|i-j\|=1$) (315)	0.009
short range ($\|i-j\|=2-4$) (116)	0.011
long range ($\|i-j\|>4$) (486)	0.008
hydrogen bond distances (122) (Å)	0.003
Ca^{2+}/ligand distances (17) (Å)	0.025
dihedral angles (78) (deg)	0.050
Average rms Deviations from Idealized Covalent Geometry	
bonds (Å)	0.013
angles (deg)	2.0
Ramachandran Plot Statistics	
residues in most favored regions	81.2%
residues in additionally allowed regions	17.6%
residues in generously allowed regions	1.1%
residues in disallowed regions	0.1%

Average rms Deviations of Atomic Coordinates (Å)

	among	vs X-ray
backbone residues 143−263	0.49	0.73
heavy-atom residues 143−263	1.05	1.40[b]
backbone residues 170−180, 230−240	0.42	0.72
heavy-atom residues 170−180, 230−240	1.04	1.66

[a] Rms deviations from experimental distance restraints and idealized geometry were calculated as averages over the 20 simulated annealing structures with the lowest violations. All 20 structures had 0 or 1 interproton distance violation above 0.3 Å, and there were no systematic violations above 0.2 Å. All Ca^{2+}−ligand distance restraint violations were smaller than 0.08 Å. There were no dihedral angle violations larger than 2°. Ramachandran plot statistics were calculated with the program PROCHECK (*30*). Rms deviations of atomic coordinates were calculated as an average over pairwise comparisons among the 20 simulated annealing structures (Among) and over pairwise comparisons between each of the 20 structures and the structure of the Ca^{2+}-free C_2A domain determined by X-ray diffraction (vs X-ray). Residues 143−263 correspond to most of the domain excluding three residues at the N-terminus and four at the C-terminus, which were disordered. Residues 170−180 and 230−240 correspond to loops 1 and 3, respectively. [b] Excluding the side chains of K189, K190, K191, and K192, which were not observable in the crystal structure.

sponding Ca^{2+} ions yielded almost final Ca^{2+}-bound structures. In these structures, we observed that the L171 carbonyl oxygen was often close to Ca2 and that one of the two D232 side-chain oxygens was often close to Ca1 (in about 50% of the structures). Including restraints to force these interactions resulted in lower overall restraint violations. This correlated with the observation that, in general, lower restraint violations were observed in the structures obtained including Ca^{2+} ions than those obtained without them, indicating that forcing the molecule toward the correct Ca^{2+}-binding mode also drives it toward a structure more consistent with all of the NMR data. Thus, we kept the L171 CO/Ca2 and D232 OD/Ca1 restraints in our final structure calculations.

The restraints forcing Ca^{2+} ions, which were set at a Ca/O distance of 2.8 Å, were all well-accommodated in the structure calculations, with the largest violations always below 0.1 Å. The restraints had very minor effects on the structures obtained without Ca^{2+} ions, with the main differences being a better convergence in the conformations of the side chains involving Ca^{2+} ligands. Thus, the overall consistency of the data yield strong support for the validity of the final Ca^{2+}-binding mode obtained (Figure 5A). The validity of this Ca^{2+}-binding mode is also supported by the good correlations observed between Mn^{2+}-induced relaxation effects on ^1H-^{15}N HSQC cross-peaks and amide proton/Ca^{2+} ion distances calculated from the structures (*24*). In addition, the only site observed by X-ray diffraction (site Ca1, ref *18*) had a coordination sphere very similar to that described here.

The three Ca^{2+} ions bind in a tight cluster at the tip of the C_2A domain (Figure 3C). The average Ca1−Ca2, Ca1−Ca3, and Ca2−Ca3 distances are 3.2, 6.0, and 4.1 Å, while the long axis of the domain spans 50 Å. The Ca1−Ca2 and Ca2−Ca3 distances are similar to the values of about 4 Å observed in binary Ca^{2+}-binding sites (*31*), although the former is considerably shorter. As seen in Figure 5B, the positions of the Ca^{2+} ions are in general well-defined, although some heterogeneity is observed for Ca3. This is likely to be a consequence of the fact that only 5 ligands are coordinating this ion (Figure 5A). The Ca1 and Ca2 sites have six ligands each. Presumably, water molecules fill the sites remaining to complete the heptacoordination sphere characteristic of Ca^{2+} ions, but these sites could be occupied by target molecules that interact with the C_2A domain in a Ca^{2+}-dependent manner such as syntaxin and phospholipids. Incomplete coordination spheres were also observed for the Ca^{2+} ions bound to the C_2 domain of PLC-δ1 (*21*) and $cPLA_2$ (*22*). This feature is thus likely to be a general property of C_2 domains.

For the C_2 domains of PLC-δ1 and $cPLA_2$, Ca^{2+} binding was observed at site Ca1 and at a site that we will refer to as Ca4. This site corresponds approximately to a cavity formed by the side chains of D172, T176, and D178 in the structure of the C_2A domain (Figure 5A). However, we did not observe Ca^{2+} binding to this site (*24*). While Ca^{2+} did not bind to site Ca2 or Ca3 in the PLC-δ1 C_2 domain, La^{3+} did bind to site Ca2 (*21*). In Figure 5C we show a superposition of residues 706−714 from the La^{3+}-bound structure of the PLC-δ1 C_2 domain with the homologous residues (230−238) of the Ca^{2+}-bound solution structure of the synaptotagmin I C_2A domain. This loop (loop 3) provides most of the ligands for sites Ca2 and Ca3 and has a remarkably similar structure in these two C_2 domains. The position of the La^{3+} in the PLC-δ1 C_2 domain is very similar to that of the Ca^{2+} ion in site Ca2 of the synaptotagmin I C_2A domain. In addition, the side chains and the carbonyl group that coordinate site Ca3 are in very similar orientations in both C_2 domains. Note that metal ion binding to this site in the PLC-δ1 C_2 domain may not have been observed because of its very low affinity, which presumably increases considerably in the presence of phospholipids (*24*). These observations strongly support our proposal that the complete Ca^{2+}-binding mode of the PLC-δ1 C_2 domain involves four Ca^{2+} ions (*24*) and emphasize the unique Ca^{2+}-binding properties of C_2 domains in general.

DISCUSSION

Ligand-induced conformational changes in proteins have provided beautiful examples of how some biological functions are executed in nature. For instance, such conformational changes have been described for Ca^{2+}-binding proteins of the EF-hand family such as calmodulin (*32*, *33*) and troponin C (*34*), where Ca^{2+} binding exposes large hydrophobic surfaces that bind target proteins. In recoverin,

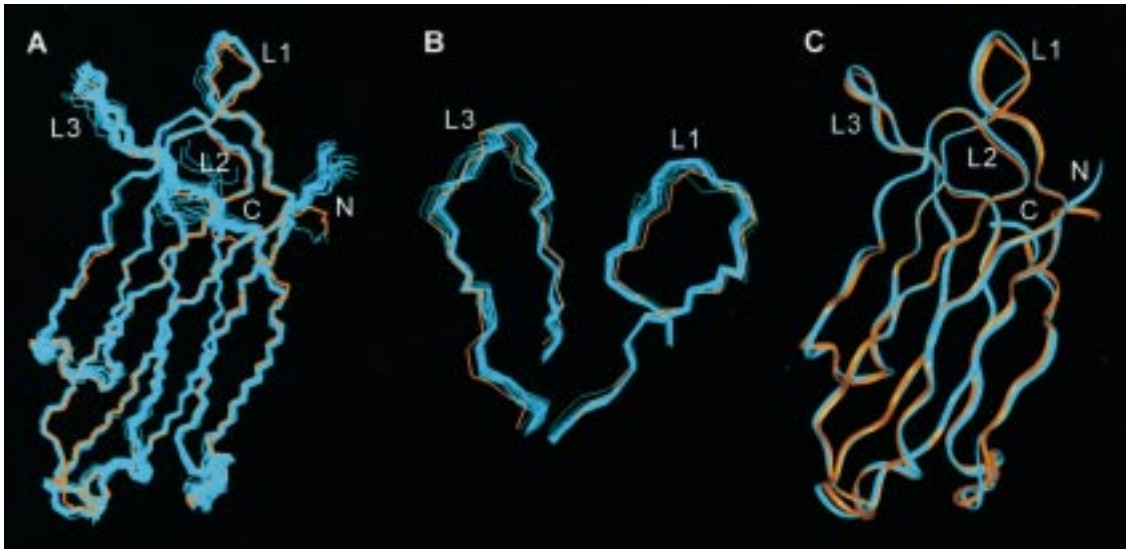

FIGURE 4: Comparison of the Ca^{2+}-bound solution structure of the C_2A domain with its Ca^{2+}-free crystal structure. (A, B) Backbone superpositions of the 20 simulated annealing structures (thin cyan lines) compared to the Ca^{2+}-free crystal structure (thick oranges lines). In A, residues 143−263 of the 20 simulated annealing structures and of the crystal structure were superimposed to the average NMR structure [all residues (140−267) are shown for the NMR structures, and all observable residues (140−265) are shown for the crystal structure]. In B, the backbones of residues 170−180 (loop 1) and 230−240 (loop 3) of the 20 simulated annealing structures and of the crystal structure were superimposed with the average NMR structure (only these residues shown). (C) Ribbon superposition of the average NMR structure (cyan) with the crystal structure (orange). The positions of loops 1−3 (labeled L1−L3) and the N- and C-termini are indicated.

another EF-hand protein, Ca^{2+} causes extrusion of a myristoyl group that is sequestered in a deep hydrophobic pocket in the absence of Ca^{2+} (*35*). Other EF-hand proteins such as S100B exhibit smaller but still significant Ca^{2+}-induced conformational changes that expose hydrophobic regions (*36*). Hence, it is always tempting to attribute Ca^{2+}-regulation of the function of a protein to a Ca^{2+}-induced conformational change. C_2 domains have, however, very different structural characteristics compared to proteins from the EF-hand family. Similarly to these proteins, C_2 domains bind multiple Ca^{2+} ions but the ions bind in a small region at the tip of a β-sandwich scaffold rather than each Ca^{2+} ion binding to a different α-helical domain. It is thus not surprising if C_2 domains function by a completely different mechanism.

The results described here demonstrate that the solution structure of the C_2A domain of synaptotagmin I saturated with Ca^{2+} is very similar to the Ca^{2+}-free crystal structure of this domain. The NMR data obtained in the absence of Ca^{2+} show that, while the structure observed in the crystals is likely to be the most populated in solution in the absence of Ca^{2+}, the structure is less stable than in the Ca^{2+}-bound form. This correlates with the observation of large temperature factors for the Ca^{2+}-binding loops in the crystal structure (*18*). Structural instability in these loops can be attributed to electrostatic repulsion among the cluster of aspartate side chains that participates in Ca^{2+} binding. Such repulsion disappears upon Ca^{2+} binding. The main structural consequence of Ca^{2+} binding is thus to rotate the aspartate side chains into the right orientations and to stabilize the structure in the region. Such structural stabilization is also indicated by the observation of a 19 °C increase in denaturation temperature upon Ca^{2+} binding (*23*). While the change from a less-defined structure to a better-defined structure could in principle be called a "conformational change", it is very different from the common use of this term which usually refers to a change from a well-defined conformation to a significantly different well-defined conformation.

The immediate question that arises is the following: can structural stabilization account in itself for the change in affinity of the C_2A domain for target molecules upon Ca^{2+} binding? This seems unlikely in the case of the Ca^{2+}-dependent interaction of the C_2A domain with syntaxin since the preferred structure of the C_2A domain, while unstable, is available in the absence of Ca^{2+} but there is no binding whatsoever between the two proteins even at 0.5 mM protein concentration (*11*). In fact, this observation is not surprising. There is a dramatic change in the electrostatic potential of the C_2A domain upon Ca^{2+} binding (*11*, *24*) and it would be surprising if a protein that binds to the highly positively charged surface of the Ca^{2+}-bound C_2A domain also had some (even weak) affinity for the negatively charged surface of the Ca^{2+}-free C_2A domain. The importance of electrostatic interactions has been demonstrated for the Ca^{2+}-dependent binding of the C_2A domain to both syntaxin (*11*) and phospholipids (*25*), and it is thus evident that these interactions play a role in the mechanism of C_2A domain function. The observation that the coordination spheres of the three Ca^{2+} ions bound to the C_2A domain are not complete indicates that an additional effect of Ca^{2+} is to provide coordination sites for the target molecules. Hydrophobic interactions involving exposed side chains such as those of M173 and F234 may also contribute to bind syntaxin and phospholipids, but they are clearly not sufficient for such binding in the absence of Ca^{2+}. The key point is that the Ca^{2+}-dependent interactions of the C_2A domain can be simply rationalized without invoking a conformational change. The "nonconformationally driven" mechanism of these interactions is made possible by the striking ability of the C_2A domain to bind three Ca^{2+} ions in a very small region at the tip of its stable β-sandwich structure.

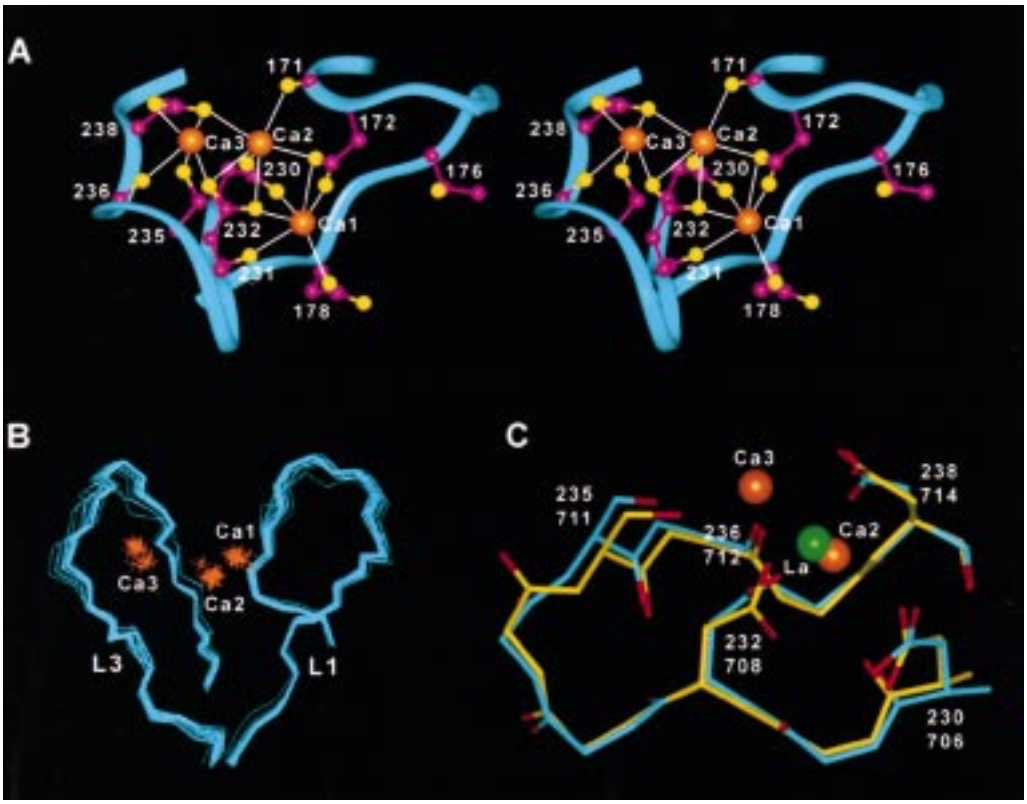

FIGURE 5: Ca^{2+}-binding mode of the C_2A domain. (A) Stereo diagram of the complete Ca^{2+}-binding mode. Only the following atoms are shown: Cα and side-chain heavy atoms of the residues involved in Ca^{2+} binding and of T176; the three carbonyl groups involved in Ca^{2+} binding; and the three Ca^{2+} ions. The backbone is represented by a ribbon (cyan). Ca^{2+} ions are colored in orange, oxygen atoms in yellow, and carbon atoms in magenta. The Ca^{2+} ions have been labeled as Ca1, Ca2, and Ca3, and the positions of the relevant residues have been labeled with the corresponding residue number. Solid white lines indicate the ligands for each Ca^{2+} ion (for Ca1, D172 OD1, D172 OD2, D178 OD1, D230 OD1, F231 O, and D232 OD1; for Ca2, L171 O, D172 OD2, F230 OD2, D232 OD1, D232 OD2, and D238 OD1; for Ca3, D232 OD2, S235 OG, K236 O, D238 OD1, and D238 OD2). (B) Backbone superposition of residues 170−180 (loop 1) and 230−240 (loop 3) of the 20 simulated annealing structures of the Ca^{2+}-bound C_2A domain with the positions of the Ca^{2+} ions shown in orange. (C) Comparison of the structure of loop 3 in the Ca^{2+}-bound C_2A domain of synaptotagmin I with the structure of the same loop in the La^{3+} complex of the PLC-δ1 C_2 domain (*21*). The backbone atoms and carbonyl oxygens of residues 230−238 of the average structure of the synaptotagmin I C_2A domain (yellow) and of residues 706−714 of the PLC-δ1 C_2 domain (cyan), as well as the side chains involved in binding to sites Ca2 and Ca3, are shown (all oxygen atoms are colored red). The backbone atoms of these 9 residues were superimposed (rms deviation 0.39 Å). Also shown are the Ca^{2+} ions bound to sites Ca2 and Ca3 of the synaptotagmin I C_2A domain (orange spheres) and the La^{3+} ion bound to site Ca2 of the PLC-δ1 C_2 domain (green sphere). The residues of loop 3 involved in metal ion binding have been labeled with the residue number (synaptotagmin I C_2A domain above; PLC-δ1 C_2 domain below).

Is the mechanism of action of the synaptotagmin I C_2A domain generally applicable to other C_2 domains? Insights to answer this question can be gained from the structures of PLC-δ1. PLC-δ1 structures were obtained from cubic and triclinic crystal forms, and after diffusing Ca^{2+}, Ba^{2+}, and La^{3+} into the former (*21*) and Sm^{3+} into the latter (*20*). All of these ions bound to sites Ca1 and Ca4, but only La^{3+} bound to site Ca2. The structural similarity in loop 3 between the Ca^{2+}-bound solution structure of the C_2A domain and the La^{3+}-bound structure of the PLC-δ1 C_2 domain, including the orientation of the ligands that form site Ca3 (Figure 5C), strongly suggests that the complete Ca^{2+} binding mode of the PLC-δ1 C_2 domain involves four Ca^{2+} ions and at the same time that binding to site Ca3 would not involve any conformational change. Thus, the La^{3+}-bound structure provides almost certainly a good representation of the fully Ca^{2+}-bound structure of the PLC-δ1 C_2 domain. The conformation of this loop in the La^{3+} complex is in fact very similar to that observed in the apo structures (and in the Ca^{2+} and Ba^{2+} complexes), showing that metal−ion binding does not change the conformation of loop 3 in the PLC-δ1 C_2 domain. The observation of different conformations of this loop in the Sm^{3+} complex (*20*) must be considered an artifact caused by crystal contacts. The structure of loop 1 exhibits much higher heterogeneity than that of loop 3 when all of the PLC-δ1 structures are compared, and it appears that this loop has some flexibility even after Ca^{2+} binding. In most structures, loop 1 occupies approximately the same region of space except for one of the molecules in the asymmetric unit of the cubic apo-PLC-δ1 where this loop adopts a more closed conformation. On the basis of this structure and of the Sm^{3+}-bound structure, a model whereby Ca^{2+} opens the conformation of loops 1 and 3 was proposed (*20, 27*) but the remaining structures of the PLC-δ1 C_2 domain provide overwhelming evidence against this model. The high-temperature factors and missing electronic density at the Ca^{2+}-binding region in the apo structures of the PLC-δ1 C_2 domain (*19, 20*) demonstrate that there is conformational flexibility in the absence of Ca^{2+}, as observed for the synaptotagmin I C_2 domain. The decrease in temperature factors after partial metal−ion binding and the resulting structures indicate that Ca^{2+} binding also causes structural stabilization although loop 1 probably remains flexible. As observed for the C_2A domain, the Ca^{2+} ions bound to the

PLC-δ1 C_2 domain also have empty coordination sites.

The above observations suggest that the synaptotagmin I C_2A domain and the PLC-δ1 C_2 domain act by a similar mechanism. For the cPLA$_2$ C_2 domain, Ca^{2+} binding causes changes in tryptophan fluorescence that suggest a conformational change (*37*). It is possible that structural stabilization might also explain the fluorescence changes or that this C_2 domain indeed acts by a different mechanism that involves a conformational change. The structure of the cPLA$_2$ C_2 domain indicates that hydrophobic interactions may play an important role in binding to phospholipids (*22*). Electrostatic interactions may still play a role in increasing the phospholipid affinity of the cPLA$_2$ C_2 domain, but a predominace of hydrophobic interactions may require that the hydrophobic regions of the loops be kept apart in the absence of Ca^{2+} to avoid lipid binding.

The role of the C_2A domain of synaptotagmin I in synaptic vesicle exocytosis is likely to be associated with its Ca^{2+}-dependent interactions with syntaxin and/or with phospholipids. A mechanism of action for the C_2A domain based on an electrostatic switch may be more suitable for its function than a Ca^{2+}-induced conformational change. After docking to the plasma membrane, synaptic vesicles are believed to undergo a priming reaction that makes them ready for fusion but fusion does not occur in the absence of Ca^{2+}; upon Ca^{2+} influx, fusion occurs very fast, within 300 μs or less (*2*). Since conformational changes are associated with slow on rates for ligand binding, the fact that the C_2A domain structure is "ready" for Ca^{2+} binding may facilitate its fast action in triggering the events that lead to membrane fusion. The electrostatic properties of the C_2A domain structure may play a role in hindering fusion before Ca^{2+} influx, because of repulsion with the highly negatively charged protein syntaxin, and in triggering fusion after Ca^{2+}-influx by binding Ca^{2+} and then attracting syntaxin. This electrostatic switch model may also be valid for many C_2 domains and is made possible by their unique Ca^{2+}-binding properties.

MATERIALS AND METHODS

Sample Preparation. Recombinant C_2A domain of synaptotagmin I (residues 140−267) was obtained by expression in *Escherichia coli* BL21(DE3) cells as a GST fusion protein, affinity purification on glutathione agarose (Sigma), cleavage with thrombin, and final purification by gel filtration, as described (*23*). Uniform ^{15}N-labeling was achieved by growing the bacteria in minimal medium using $^{15}NH_4Cl$ as the sole nitrogen source; for uniform ^{15}N,^{13}C-labeled samples, $^{13}C_6$-glucose was used as the sole carbon source. Typical yields were 5 mg of pure protein/L of bacterial culture. Most NMR experiments were performed with 1 mM C_2A domain samples at 34 °C and pH 5.0 (40 mM perdeuterated acetate, 100 mM NaCl) using H_2O/D_2O 9:1 (v/v) as the solvent. Some homonuclear 2D spectra, the 4D ^{1}H-^{13}C,^{1}H-^{13}C HMQC−NOESY−HMQC experiment, and ^{1}H-^{15}N HSQC spectra to measure H/D exchange rates were obtained with samples dissolved in D_2O. The protein concentration in the latter experiments was 0.5 mM. Samples of the Ca^{2+}-free C_2A domain contained 0.2 mM EGTA, and samples of Ca^{2+}-bound C_2A domain contained 30 mM $CaCl_2$.

NMR Spectroscopy. Initial homonuclear and ^{15}N-edited spectra were acquired on a Varian VXR-500 spectrometer using an indirect detection probe, and all other experiments were acquired after an upgrade to a Varian Unity 500 console using a PFG-triple resonance probe. Assignment of the ^{1}H, ^{15}N, and ^{13}C resonances of the Ca^{2+}-free and Ca^{2+}-bound C_2A domains was obtained using 2D DQF−COSY (*38*), 2D TOCSY(*39*), 2D NOESY (*40*), ^{1}H-^{15}N HSQC (*41*), 3D ^{1}H-^{15}N TOCSY−HMQC, and NOESY−HMQC (*42*, *43*), and a series of triple resonance experiments incorporating pulsed field gradients, water flip-back pulses, and sensitivity enhancement when amide protons were detected in the F3 dimension (*44*): HNCO (*45*), HNCACB(*46*), (H)CBCACO(CA)HA (*47*), (H)C(CO)NH-TOCSY (*48*, *49*), and HCCH-TOCSY (*50*) spectra. Details on all these experiments have been described elsewhere (*23*, *28*, *51*). The 2D NOESY (50−120 ms mixing times) and 3D ^{1}H-^{15}N NOESY−HMQC (120 ms mixing times) spectra were also used to derive distance restraints for structure determination. All data were processed and analyzed with the program Felix (MSI). For the Ca^{2+}-bound C_2A domain, we also acquired a 4D ^{1}H-^{13}C,^{1}H-^{13}C HMQC−NOESY−HMQC experiment (*52*) using a mixing time of 100 ms. This experiment was acquired in the hypercomplex mode with 50, 15, and 15 increments in the F1 (^{1}H), F2 (^{13}C), and F3 (^{13}C) dimensions, respectively, and 256 complex points/FID. The spectral widths were 4200 (F1), 3000 (F2), 3000 (F3), and 6000 (F4) Hz. These data were processed with the program NMRPipe (*53*). After linear prediction in the F2 and F3 dimensions to double the number of points, zero filling and Fourier transformation in all dimensions, a matrix of 128 (F1) × 64 (F2) × 64 (F3) × 512 (F4) real points was obtained. Peak picking of these data was performed with the program PIPP (Dan Garrett, Laboratory of Chemical Physics, NIH). H/D exchange rates were measured from the rate of disappearance of ^{1}H-^{15}N HSQC cross-peaks after dissolving the corresponding sample in D_2O. The $^3J_{HN\alpha}$ coupling constants were measured from HNHA spectra (*54*, *55*) applying a 1.11 correction factor. These spectra were acquired in the hypercomplex mode with 64 and 32 increments in the F1 and F2 dimensions, respectively, 512 complex points per FID, and spectral widths of 7600 (F1), 5800 (F2), and 1163 (F3) Hz. Linear prediction in the F2 dimension, zero filling in all dimensions, Fourier transformation, and removal of the aliphatic part of the F3 dimension yielded matrixes of 256 (F1) × 128 (F2) × 512 (F3) real points.

Structure Calculations. Structures of the Ca^{2+}-free and Ca^{2+}-bound C_2A domains were calculated by simulated annealing (*29*) followed by energy minimization. The force constants used were 50 kcal mol^{-1} Å^{-2} and 200 kcal mol^{-1} rad^{-2} for distance and torsion angle restraints, respectively. The calculations were performed with the standard simulated annealing protocol implemented in the INSIGHTII/NMRchitect/DISCOVER suite of programs (MSI) but multiplying by 20 the force constant for chiral restraints, which were used to ensure the proper chirality in the backbone and in the threonine and isoleucine side chains. Interproton distance restraints for structure calculations were derived from the 2D NOESY and 3D ^{1}H-^{15}N NOESY−HMQC data for the Ca^{2+}-free C_2A domain, and from these data plus the 4D ^{1}H-^{13}C,^{1}H-^{13}C HMQC−NOESY−HMQC data for the Ca^{2+}-bound C_2A domain. NOE cross-peak intensities were classified as strong, medium, and weak and assigned to restraints of 1.8−2.7, 1.8−3.5 and 1.8−5.0 Å, respectively,

with standard corrections applied to the upper limits for restraints involving methyl protons, and magnetically equivalent methylene protons or isopropyl methyl groups (*56*). A separate classification was used for NOEs involving methyl groups to account for their stronger intensities. Intraresidue and sequential restraints were only used if they were conformationally significant. Phi torsion angle restraints of −10°/−90° or −80°/−160° were used for residues with $^3J_{HN\alpha}$ coupling constants smaller than 6 Hz or larger than 8 Hz, respectively. Hydrogen bond restraints were used in the final stages of refinement for amide protons with slow H/D exchange rates, with the corresponding hydrogen bond acceptor groups deduced from the initial structures calculated with NOE data alone. The H/O distances were restrained to 1.7−2.3 Å and the N/O distances to 2.7−3.3 Å. Restraints between Ca^{2+} ions and Ca^{2+} ligands were used only after structures incorporating all NOE, Hbond, and phi restraints had been calculated, and were incorporated progressively as explained in the text. The Ca−O distances were restrained to 1.8−2.8 Å. All the images shown in Figures 2−5 were created with the program INSIGHTII (MSI), except where indicated otherwise.

ACKNOWLEDGMENT

We thank Lewis Kay for providing pulse sequences for all triple resonance experiments, Lawrence McIntosh and Lewis Kay for help on setting up these experiments, and Bryan Sutton and Steve Sprang for fruitful discussions. We thank Dan Garrett for making available the program PIPP.

REFERENCES

1. Geppert, M., Goda, Y., Hammer, R. E., Li, C., Rosahl, T. W., Stevens, C. F., and Südhof, T. C. (1994) *Cell 79*, 717−727.
2. Südhof, T. C. (1995) *Nature 375*, 645−653.
3. Südhof, T. C., and Rizo, J. (1996) *Neuron 17*, 379−388.
4. Perin, M. S., Fried, V. A., Mignery, G. A., Jahn, R., and Südhof, T. C. (1990) *Nature 345*, 260−263.
5. Perin, M. S., Johnston, P. A., Özcelik, T., Jahn, R., Francke, U., and Südhof, T. C. (1991) *J. Biol. Chem. 266*, 615−622.
6. Perin, M. S., Brose, N., Jahn, R., and Südhof, T. C. (1991b) *J. Biol. Chem. 266*, 623−629.
7. Brose, N., Petrenko, A. G., Südhof, T. C., and Jahn, R. (1992) *Science 256*, 1021−1025.
8. Davletov, B. A., and Südhof, T. C. (1993) *J. Biol. Chem. 268*, 26386−26390.
9. Li, C., Ullrich, B., Zhang, J. Z., Anderson, G. W., Brose, N., and Südhof, T. C. (1995) *Nature 375*, 594−599.
10. Kee, Y., and Scheller, R. H. (1996) *J. Neurosci. 16*, 1975−1981.
11. Shao, X., Li, C., Fernandez, I., Zhang, X., Südhof, T. C., and Rizo, J. (1997) *Neuron 18*, 133−142.
12. Scheller, R. H. (1995) *Neuron 14*, 893−897.
13. Heidelberger, R., Heinemann, C., Neher, E., and Mathews, G. (1994) *Nature 371*, 513−515.
14. Nishizuka, Y. (1988) *Nature 334*, 661−665.
15. Brose, N., Hofmann, K., Hata, Y., and Südhof, T. C. (1995) *unc-13* gene define novel family of C_2-domain proteins. *J. Biol. Chem. 270*, 25273−25280.
16. Nalefski, E. A., and Falke, J. J. (1996) *Protein Sci. 5*, 2375−2390.
17. Rizo, J., and Südhof, T. C. (1998) *J. Biol. Chem. 273*, 15879−15882.
18. Sutton, R. B., Davletov, B. A., Berghuis, A. M., Südhof, T. C., and Sprang, S. R. (1995) Structure of the first C_2 domain of synaptotagmin I: a novel Ca^{2+}/phospholipid-binding fold. *Cell 80*, 929−938.
19. Essen, L.-O., Perisic, O., Cheung, R., Katan, M., and Williams, R. L. (1996) *Nature 380*, 595−602.
20. Grobler, J. A., Essen, L. O., Williams, R. L., and Hurley, J. H. (1996) *Nat. Struct. Biol. 3*, 788−795.
21. Essen, L.-O., Perisic, O., Lynch, D. E., Katan, M., and Williams, R. L. (1997) *Biochemistry 36*, 2753−2762.
22. Perisic, O., Fong, S., Lynch, D. E., Bycroft, M., and Williams, R. L. (1998) *J. Biol. Chem. 273*, 1596−1604.
23. Shao, X., Davletov, B. A., Sutton, R. B., Südhof, T. C., and Rizo, J. (1996) *Science 273*, 248−251.
24. Ubach, J., Zhang, X., Shao, X., Südhof, T. C., and Rizo, J. (1998) *EMBO J. 17*, 3921−3930.
25. Zhang, X., Rizo, J., and Südhof, T. C. (1998) *Biochemistry 37*, 12395−12403.
26. Newton, A. (1995) *Curr. Biol. 5*, 973−976.
27. Grobler, J. A., and Hurley, J. H. (1997) *Nat. Struct. Biol. 4*, 261−262.
28. Shao, X., Südhof, T. C., and Rizo, J. (1997) *J. Biomol. NMR 10*, 307−308.
29. Nilges, M., Clore, G. M., and Gronenborn, A. M. (1988) *FEBS Lett. 239*, 129−136.
30. Laskowski, R. A., MacArthur, M. W., Moss, D. S., and Thornton, J. M. (1993) *J. Appl. Crystallogr. 26*, 283−291.
31. Emsley, J., et al. (1994) *Nature 367*, 338−345.
32. Zhang, M., Tanaka, T., and Ikura, M. (1995) *Nat. Struct. Biol. 2*, 758−767.
33. Kuboniwa, H., Tjandra, N., Grzesiek, S., Ren, H., Klee, C. B., and Bax, A. (1995) *Nat. Struct. Biol. 2*, 768−776.
34. Gagné, S. M., Tsuda, S., Li, M. X., Smillie, L. B., and Sykes, B. D. (1995) *Nat. Struct. Biol. 2*, 784−789.
35. Ames, J. B., Ishima, R., Tanaka, T., Gordon, J. I., Stryer, L., and Ikura, M. (1997) *Nature 389*, 198−202.
36. Smith, S. P., and Shaw, G. S. (1998) *Structure 6*, 211−222.
37. Nalefski, E. A., Slazas, M. M., and Falke, J. J. (1997) *Biochemistry 36*, 12011−12018.
38. Rance, M., Sørensen, O. W., Bodenhausen, G., Wagner, G., Ernst, R. R., and Wüthrich, K. (1983) *Biochem. Biophys. Res. Commun. 117*, 479−485.
39. Davis, D. G., and Bax, A. (1985) *J. Am. Chem. Soc. 107*, 2820−2821.
40. Kumar, A., Wagner, G., Ernst, R. R., and Wüthrich, K. (1981) *J. Am. Chem. Soc. 103*, 3654−3658.
41. Bodenhausen, G., and Ruben, D. J. (1980) *Chem. Phys. Lett. 69*, 185−199.
42. Marion, D., Kay, L. E., Sparks, S. W., Torchia, D. A., and Bax, A. (1989) *J. Am. Chem. Soc. 111*, 1515−1517.
43. Marion, D., Driscoll, P. C., Kay, L. E., Wingfield, P. T., Bax, A., Gronenborn, A. M., and Clore, G. M. (1989) *Biochemistry 28*, 6150−6156.
44. Zhang, O., Kay, L. E., Olivier, J. P., and Forman-Kay, J. (1994) *J. Biomol. NMR 4*, 845−858.
45. Kay, L. E., Xu, G. Y., and Yamazaki, T. (1994) *J. Magn. Reson., Ser. A 109*, 129−133.
46. Muhandiram, D. R., and Kay, L. E. (1994) *J. Magn. Reson., Ser. B 103*, 203−216.
47. Kay, L. E. (1993) *J. Am. Chem. Soc. 115*, 2055−2057.
48. Grzesiek, S., Anglister, J., and Bax, A. (1993) *J. Magn. Reson., Ser. B 101*, 114−119.
49. Logan, T. M., Olejniczack, E. T., Xu, R. X., and Fesik, S. W. (1993) *J. Biomol. NMR 3*, 225−231.
50. Kay, L. E., Xu, G.-Y., Singer, A. U., Muhandiram, D. R., and Forman-Kay, J. D. (1993) *J. Magn. Reson., Ser. B 101*, 333−337.
51. Rizo, J., Liu, Z.-P., and Gierasch, L. M. (1994) *J. Biomol. NMR 4*, 741−760.
52. Clore, G. M., Lay, L. E., Bax, A., and Gronenborn, A. M. (1991) *Biochemistry 30*, 12−18.
53. Delaglio, F., Grzesiek, S., Vuister, G. W., Zhu, G., Pfeifer, J., and Bax, A. (1995) *J. Biomol. NMR 6*, 277−293.
54. Vuister, G. W., and Bax, A. (1993) *J. Am. Chem. Soc. 115*, 7772−7777.

55. Kuboniwa, H., Grzesiek, S., Delaglio, F., and Bax, A. (1994) *J. Biomol. NMR 4*, 871−878.
56. Wüthrich, K. (1986) *NMR of proteins and nucleic acids*, John Wiley & Sons, Inc., New York.
57. Kraulis, P. J. (1991) MOLSCRIPT: a program to produce both detailed and schematic plots of protein structures. *J. Appl. Crystallogr. 24*, 946−950.
58. Merritt, E. A., and Murphy, M. E. P. (1994) *Acta Crystallogr., Sect. D 50*, 869−873.

BI981789H